Photonics-Assisted Super-Octave Microwave Phase Shifter
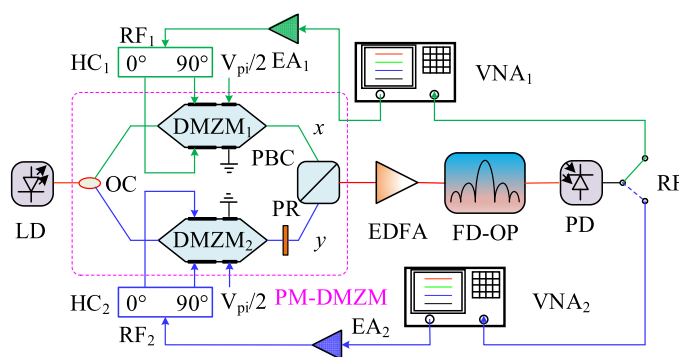
Mingzheng Lei
Zhennan Zheng
Jinwang Qian
Mutong Xie
Xinlu Gao
Shanguo Huang

Photonics-Assisted Super-Octave Microwave Phase Shifter

Mingzheng Lei , **Zhennan Zheng, Jinwang Qian, Mutong Xie,**
Xinlu Gao , **and Shanguo Huang**

State Key Laboratory of Information Photonics and Optical Communications, Beijing
University of Posts and Telecommunications, Beijing 100876, China

Abstract: A photonics-assisted super-octave microwave phase shifter is proposed. The super-octave frequency range is achieved by eliminating the second-order distortions (SDs) with the techniques of polarization interleaving and second-order optical sidebands (2-OSBs) phase processing. Polarization interleaving is based on a polarization-multiplexing dual-drive Mach-Zehnder modulator (PM-DMZM) and single sideband with carrier (SSB+C) modulation. 2-OSBs phase processing is implemented by introducing opposite phase shifts to the $\pm$2-OSBs in a Fourier-domain optical processor (FD-OP). The proposed phase shifter is experimentally verified by proof-of-concept experiments. Experimental results show that flat phase shifts cover a full 360° range with less than 3-dB power variation over 11.5-25 GHz. Besides, excellent long-term stability is presented with a maximum phase/power fluctuation of only 1.49°/0.57 dB. Compared with the conventional FD-OP-based photonic microwave phase shifter, the proposed one improves the second-order spurious free dynamic range ($SFDR_2$) by 13.57 dB.

Index Terms: Phase shifter, radio frequency photonics, optical signal processing, spurious free dynamic range.

1. Introduction

Microwave phase shifter is one of the most essential components in phased array beamforming, phase coding, microwave filters, phase noise measurement, linear frequency modulated signals generation, and interference cancellation [1]–[5]. Conventional electrical phase shifters suffer from limited phase-shifting range [6]–[8], limited frequency-operating range [6], [8], limited phase-tuning resolution [6]–[9], and frequency-dependent phase shifts [7], [8]. In recent years, photonics-assisted microwave phase shifters have been reported based on different techniques such as stimulated Brillouin scattering [10], polarization maintaining fiber Bragg grating [11], highly nonlinear fiber [12], parallel modulators [13], polarization-dependent modulator [14], [15], and Fourier-domain optical processor (FD-OP) [16], [17]. Compared with pure RF phase shifters, the photonics-assisted ones have the advantages of immunity to electromagnetic interference [10]–[18], full 360° phase shifts [10]–[17], large bandwidth [10]–[18], high resolution and good system flexibility due to programmable optical signal processor [16], [17]. However, these optically-controlled microwave phase shifters do not support super-octave applications due to the spectra overlapping between

fundamental signals and their second-order distortions (SDs) [19], [20]. SDs include second-order intermodulation distortion (IMD2) and second-order harmonic distortion (SHD). They are non-ignorable when the input RF powers are large enough. Such spectra overlapping deteriorates the signal-to-noise ratio (SNR) and reducing the phase shifting accuracy. Furthermore, SDs are dominant in contrast to third-order intermodulation distortion (IMD3) when input RF powers are not very large [19]–[21], which means that the threshold of spurious free dynamic range (SFDR) is limited by second-order SFDR ($SFDR_2$) rather than third-order SFDR ($SFDR_3$) in super-octave links.

To suppress SDs, the most commonly used method is differential detection [19], [20], [22]. In this method, a balanced photodetector (BPD) is used to recover the RF signal. The SDs recovered by the two sub-photodetectors (sub-PDs) inside the BPD are in phase, resulting in self-cancel of SDs after BPD. However, additional calibration is required for this method because the two path lengths before the BPD need to be accurately matched. Another method to suppress SDs is based on a polarization-sensitive phase modulator (PM) [21]. By carefully adjusting the polarization states, the SDs recovered from two orthogonally polarized directions are complementary. The third method to suppress SDs is utilizing a polarization-multiplexing dual-parallel Mach-Zehnder modulator (PM-DPMZM) [23]. By carefully biasing the PM-DPMZM, the SDs recovered from the two sub-MZMs inside each sub-DPMZM are out of phase. However, such three methods fail in phase-shifting photonic links, because the phases of SDs are also shifted. The shifted phases break the phase conditions of SDs suppression. Suppressing SDs in super-octave phase-shifting photonic links is of great importance, but few works have been reported.

In this paper, we propose a photonics-assisted super-octave microwave phase shifter based on polarization interleaving and second-order optical sidebands (2-OSBs) phase processing. Polarization interleaving is realized by single sideband with carrier (SSB+C) modulation on a polarization-multiplexing dual-drive Mach-Zehnder modulator (PM-DMZM). Interleaving the signals in polarization domain can get rid of the interference between first-order optical sidebands (1-OSBs) and zeroth-order optical sidebands (0-OSBs). Thus, different phase shifts can be added to 1-OSBs without introducing interference to 0-OSBs. SBB+C modulation avoids SHDs that originate from the beating between $\pm$1-OSBs. After introducing opposite phase shifts to $\pm$2-OSBs using an FD-OP, SDs with the same frequencies cancel out each other in PD. Therefore, the proposed phase shifter is free from interference of SDs in a super-octave frequency range. Besides, the proposed phase shifter has better stability than the methods in [19]–[23] in terms of SDs suppression, because it does not need accurate path length adjustment, stable polarization monitoring, or complex bias voltage control. The rest of the paper is arranged as follows: in Section 2 we provide theoretical analysis for the proposed shifter; in Section 3, proof-of-concept experiments are carried out, and results are discussed; finally, conclusions are drawn in Section 4.

2. Principle

The schematic diagram of the proposed super-octave photonic microwave phase shifter is shown in Fig. 1. A continuous wave with an angular frequency of ω from a laser diode (LD) is fed into a PM-DMZM. The PM-DMZM consists of a 3-dB optical coupler (OC), two DMZMs, a polarization rotator (PR), and a polarization beam combiner (PBC). A super-octave signal is converted into two sub-octave signals (RF_1 and RF_2) by a bandwidth allocation block. The bandwidth allocation of the super-octave signal can be realized through the block presented in [24] together with an analog-digital converter, through a 3-dB electrical coupler and two electrical filters with different operational bandwidths, or through more than one signal generators. The optical spectra of the two sub-octave signals are shown in Figs. 1(a) and 1(b), where $f_3 > 2f_1$, $f_2 - f_1 < f_1$, and $f_3 - f_2 < f_1$. According to the relationship among f_1, f_2, and f_3, we have $f_3 < 3f_1$, namely the highest frequency is less than three times the lowest frequency. The two arms of $DMZM_1$ are driven by RF_1 via a 90° hybrid coupler (HC_1), and the two arms of $DMZM_2$ are driven by RF_2 via a 90° HC (HC_2). Both of the two DMZMs are biased at quadrature transmission point to implement SSB+C modulation.
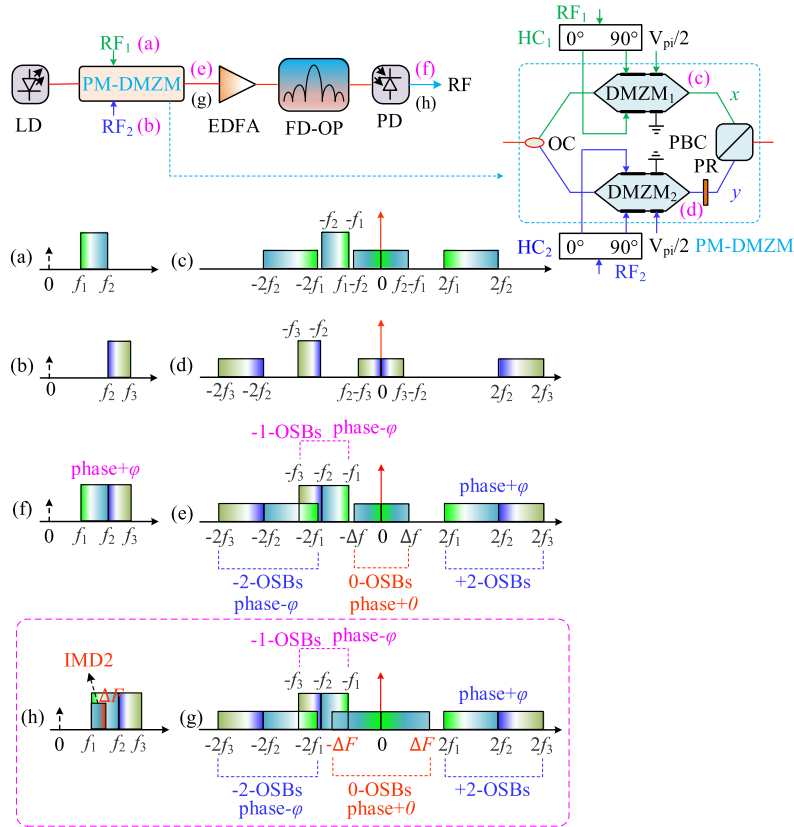
Fig. 1. Schematic diagram of the proposed super-octave photonic microwave phase shifter; detailed layout of the PM-DMZM; spectrum evolution of (a), (b), (f) electrical and (c)–(e) optical signals with frequency division; and spectrum evolution of (h) electrical and (g) optical signals without frequency division. LD: laser diode, PM-DMZM: polarization-multiplexing dual-drive Mach-Zehnder modulator, OC: optical coupler, PR: polarization rotator, PBC: polarization beam combiner, HC: hybrid coupler, EDFA: erbium-doped fiber amplifier, FD-OP: Fourier-domain optical processor, PD: photodetector. The frequencies in (c)–(e), and (g) are frequency offsets relative to the optical carrier.

As a result, the +1-OSBs are suppressed, as shown in Figs. 1(c) and 1(d). To analyze the SDs suppression, two-tone analysis is undertaken. At the output of the two DMZMs, the optical fields are expressed as

$$
\begin{aligned}
E_1 &\propto \exp\left\{jm[\sin(\omega_1 t) + \sin(\omega_3 t)]\right\} \exp(j\omega t) \\
&+ \exp\left\{jm[\cos(\omega_1 t) + \cos(\omega_3 t)]\right\} \exp\left(j\omega t + j\frac{\pi}{2}\right)
\end{aligned}
\tag{1}
$$

$$
\begin{aligned}
E_2 &\propto \exp\left\{jm[\sin(\omega_2 t) + \sin(\omega_4 t)]\right\} \exp(j\omega t) \\
&+ \exp\left\{jm[\cos(\omega_2 t) + \cos(\omega_4 t)]\right\} \exp\left(j\omega t + j\frac{\pi}{2}\right)
\end{aligned}
\tag{2}
$$

where m is the modulation index; $\omega_{1,3}$ ($2\pi f_1 \leq \omega_1 < \omega_3 < 2\pi f_2$) and $\omega_{2,4}$ ($2\pi f_2 \leq \omega_2 < \omega_4 < 2\pi f_3$) are angular frequencies of the RF signals added to DMZM$_{1,2}$. A 90° PR followed with the DMZM$_2$ rotates the polarization state of the optical signal by 90°. Hence the two optical signals from the two DMZMs are orthogonally polarized. After combination by a PBC, the two orthogonally polarized optical signals are interleaved in polarization domain. The output optical fields along the two principle

axes (x and y) of the PBC are written as

$$\begin{bmatrix} E_x \\ E_y \end{bmatrix} \propto \begin{bmatrix} E_1 \\ E_2 \exp(j\theta) \end{bmatrix} \tag{3}$$

where θ is the phase difference between E_x and E_y. The combined super-octave optical spectra are shown in Fig. 1(e), where $\Delta f = \max\{f_2 - f_1, f_3 - f_2\}$. Thanks to the structure of polarization interleaving, 1-OSBs are separated from 0-OSBs in frequency domain. The sideband order is defined as the sum of the coefficients of ω_1 and ω_3, or the sum of the coefficients of ω_2 and ω_4. The orthogonally polarized super-octave optical signals are amplified by an erbium-doped fiber amplifier (EDFA) to compensate the power loss in the link. The FD-OP mainly comprises of a conventional grating and a 2-D liquid crystal on silicon (LCoS) optical processor. The LCoS processor is a polarization-independent device which consists of a matrix of reflective liquid crystal elements. The conventional grating disperses different input optical wavelengths to different columns of the LCoS, and disperses same input optical wavelengths to different rows of the LCoS. By applying voltages to these matrix elements, reflected optical signals with different wavelengths can obtain individual phase shifts and attenuation [16], [25]. After introducing different phase shifts to different OSBs in the FD-OP, the orthogonally polarized super-octave optical signals along x- and y- directions are given by

$$
\begin{aligned}
E_x \propto \Bigg\{ &\left[J_0(m)J_2(m) \exp\left[j\left(-2\omega_1 t - \frac{\pi}{4} + \varphi_{-2}\right)\right] + J_0(m)J_2(m) \exp\left[j\left(-2\omega_3 t - \frac{\pi}{4} + \varphi_{-2}\right)\right] \right. \\
&+ J_1(m)J_1(m) \exp\left[j\left(-\omega_1 t - \omega_3 t - \frac{\pi}{4} + \varphi_{-2}\right)\right] \\
&- \sqrt{2}J_0(m)J_1(m) \exp\left[j\left(-\omega_1 t + \varphi_{-1}\right)\right] - \sqrt{2}J_0(m)J_1(m) \exp\left[j\left(-\omega_3 t + \varphi_{-1}\right)\right] \\
&+ J_1(m)J_1(m) \exp\left[j\left(\omega_1 t - \omega_3 t - \frac{3\pi}{4} + \varphi_0\right)\right] + J_0(m)J_0(m) \exp\left[j\left(\frac{\pi}{4} + \varphi_0\right)\right] \\
&+ J_1(m)J_1(m) \exp\left[j\left(\omega_3 t - \omega_1 t - \frac{3\pi}{4} + \varphi_0\right)\right] \\
&+ J_0(m)J_2(m) \exp\left[j\left(2\omega_1 t - \frac{\pi}{4} + \varphi_2\right)\right] + J_0(m)J_2(m) \exp\left[j\left(2\omega_3 t - \frac{\pi}{4} + \varphi_2\right)\right] \\
&\left. + J_1(m)J_1(m) \exp\left[j\left(\omega_1 t + \omega_3 t - \frac{\pi}{4} + \varphi_2\right)\right] \right\} \exp(j\omega t)
\end{aligned} \tag{4}
$$

$$
\begin{aligned}
E_y \propto \Bigg\{ &\left[J_0(m)J_2(m) \exp\left[j\left(-2\omega_2 t - \frac{\pi}{4} + \varphi_{-2}\right)\right] + J_0(m)J_2(m) \exp\left[j\left(-2\omega_4 t - \frac{\pi}{4} + \varphi_{-2}\right)\right] \right. \\
&+ J_1(m)J_1(m) \exp\left[j\left(-\omega_2 t - \omega_4 t - \frac{\pi}{4} + \varphi_{-2}\right)\right] \\
&- \sqrt{2}J_0(m)J_1(m) \exp\left[j\left(-\omega_2 t + \varphi_{-1}\right)\right] - \sqrt{2}J_0(m)J_1(m) \exp\left[j\left(-\omega_4 t + \varphi_{-1}\right)\right] \\
&+ J_1(m)J_1(m) \exp\left[j\left(\omega_2 t - \omega_4 t - \frac{3\pi}{4} + \varphi_0\right)\right] + J_0(m)J_0(m) \exp\left[j\left(\frac{\pi}{4} + \varphi_0\right)\right] \\
&+ J_1(m)J_1(m) \exp\left[j\left(\omega_4 t - \omega_2 t - \frac{3\pi}{4} + \varphi_0\right)\right] \\
&+ J_0(m)J_2(m) \exp\left[j\left(2\omega_2 t - \frac{\pi}{4} + \varphi_2\right)\right] + J_0(m)J_2(m) \exp\left[j\left(2\omega_4 t - \frac{\pi}{4} + \varphi_2\right)\right] \\
&\left. + J_1(m)J_1(m) \exp\left[j\left(\omega_2 t + \omega_4 t - \frac{\pi}{4} + \varphi_2\right)\right] \right\} \exp[j(\omega t + \theta)]
\end{aligned} \tag{5}
$$

where $J_n(\cdot)$ is nth-order Bessel function of the first kind; φ_n ($n = -2, -1, 0, 2$) is the phase shift introduced to nth-order optical sidebands (n-OSBs). Ignoring the DC components and the third-order distortions, the photocurrents recovered by PD are described by

$$i(t) = i_x(t) + i_y(t) \propto E_x \times E_x^* + E_y \times E_y^* \tag{6}$$

where $i_x(t)$ and $i_y(t)$ are expressed as

$$
\begin{aligned}
i_x(t) \propto\ & -\sqrt{2}J_0^3(m)J_1(m)\ \cos\left(\omega_1 t + \frac{\pi}{4} + \varphi_0 - \varphi_{-1}\right) \\
& -\sqrt{2}J_0^3(m)J_1(m)\ \cos\left(\omega_3 t + \frac{\pi}{4} + \varphi_0 - \varphi_{-1}\right) \\
& +J_0^3(m)J_2(m)\ \cos\left(2\omega_1 t + \frac{\pi}{2} + \varphi_0 - \varphi_{-2}\right) + J_0^3(m)J_2(m)\ \cos\left(2\omega_3 t + \frac{\pi}{2} + \varphi_0 - \varphi_{-2}\right) \\
& +J_0^2(m)J_1^2(m)\ \cos\left(\omega_1 t + \omega_3 t + \frac{\pi}{2} + \varphi_0 - \varphi_{-2}\right) \\
& +J_0^3(m)J_2(m)\ \cos\left(2\omega_1 t - \frac{\pi}{2} + \varphi_2 - \varphi_0\right) + J_0^3(m)J_2(m)\ \cos\left(2\omega_3 t - \frac{\pi}{2} + \varphi_2 - \varphi_0\right) \\
& +J_0^2(m)J_1^2(m)\ \cos\left(\omega_1 t + \omega_3 t - \frac{\pi}{2} + \varphi_2 - \varphi_0\right)
\end{aligned}
\tag{7}
$$

$$
\begin{aligned}
i_y(t) \propto\ & -\sqrt{2}J_0^3(m)J_1(m)\ \cos\left(\omega_2 t + \frac{\pi}{4} + \varphi_0 - \varphi_{-1}\right) \\
& -\sqrt{2}J_0^3(m)J_1(m)\ \cos\left(\omega_4 t + \frac{\pi}{4} + \varphi_0 - \varphi_{-1}\right) \\
& +J_0^3(m)J_2(m)\ \cos\left(2\omega_2 t + \frac{\pi}{2} + \varphi_0 - \varphi_{-2}\right) + J_0^3(m)J_2(m)\ \cos\left(2\omega_4 t + \frac{\pi}{2} + \varphi_0 - \varphi_{-2}\right) \\
& +J_0^2(m)J_1^2(m)\ \cos\left(\omega_2 t + \omega_4 t + \frac{\pi}{2} + \varphi_0 - \varphi_{-2}\right) \\
& +J_0^3(m)J_2(m)\ \cos\left(2\omega_2 t - \frac{\pi}{2} + \varphi_2 - \varphi_0\right) + J_0^3(m)J_2(m)\ \cos\left(2\omega_4 t - \frac{\pi}{2} + \varphi_2 - \varphi_0\right) \\
& +J_0^2(m)J_1^2(m)\ \cos\left(\omega_2 t + \omega_4 t - \frac{\pi}{2} + \varphi_2 - \varphi_0\right)
\end{aligned}
\tag{8}
$$

From Eqs. (7) and (8), the IMD2s ($\omega_3 - \omega_1, \omega_4 - \omega_2$) with the same frequencies cancel out each other and are independent of φ_n thanks to SSB+C modulation. Besides, the IMD2s ($\omega_3 - \omega_1, \omega_4 - \omega_2$) fall outside the fundamental frequencies, which can be filtered out by an electrical filter. When $\varphi_0 = 0$, the fundamental signals obtain a phase shift $-\varphi_{-1}$. If $\omega_2 = 2\omega_1$, the third and sixth terms interfere the phase shift of the first term, which eventually reduces the fundamental phase shifting accuracy. By setting $\varphi_2 = -\varphi_{-2}$, the SHDs with the same frequencies cancel out each other, and so do the IMD2s ($\omega_1 + \omega_3, \omega_2 + \omega_4$). By setting $\varphi_{-1} = \varphi_{-2} = -\varphi_2 = -\varphi$, and Eq. (6) is simplified as

$$i(t) \propto \sqrt{2}J_0^3(m)J_1(m) \sum_{i=1}^{4} \cos\left(\omega_i t - \frac{3\pi}{4} + \varphi\right) \tag{9}$$

From Eq. (9), the fundamental phases can be shifted full 360° by changing φ, and all of the SDs are suppressed, as shown in Fig. 1(f). Thus, a super-octave photonic microwave phase shifter is achieved.

Note that the proposed shifter divides the input super-octave signal into two sub-octave signals. Fig. 1(g) shows the scenario without signal frequency division. The 0-OSBs overlap with the -1-OSBs at the frequency range $[-\Delta F, -f_1]$, where $\Delta F = f_3 - f_1$. In the FD-OP, the 0-OSBs at the frequency range $[-\Delta F, -f_1]$ will obtain a phase shift $-\varphi$. After photoelectric conversion in a PD, the IMD2s at the frequency range $[f_1, \Delta F]$ fall into fundamental frequencies and cannot be filtered out, as
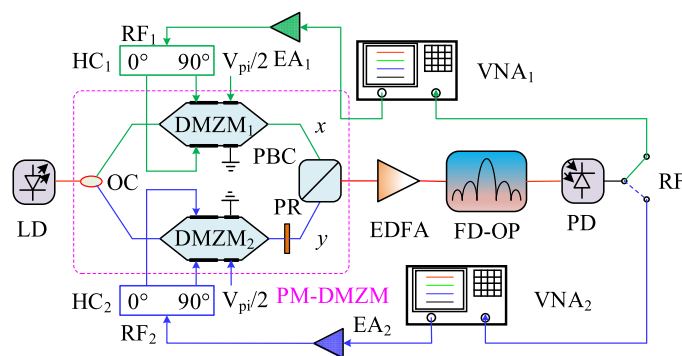
Fig. 2. Experimental set-up of the proposed super-octave photonic microwave phase shifter. EA: electrical amplifier, VNA: vector network analyzer.
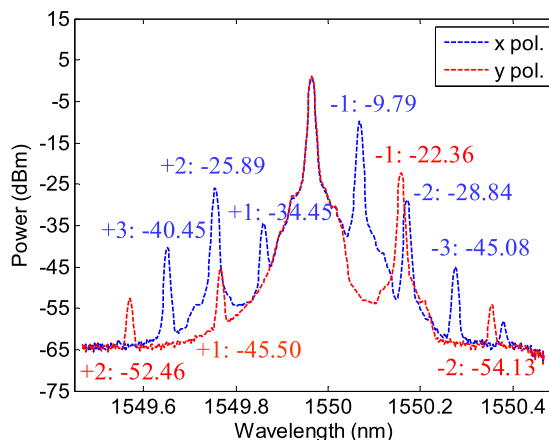

Fig. 3. The output optical spectra of the PM-DMZM along x- (blue) and y- (red) directions.

shown in Fig. 1(h). The obtained phase shift $-\varphi$ breaks the phase conditions of IMD2s suppression, eventually deteriorating the SNR and reducing the fundamental phase shifting accuracy.

3. Experimental Results and Discussion

To demonstrate the performance of phase tuning and SDs suppression, proof-of-concept experiments are conducted using the set-up shown in Fig. 2. A 12-dBm continuous optical wave at 1550 nm from an LD (Coherent Solutions LaserBlade) is coupled into a PM-DMZM (Fujitsu FTM7980EDA). The RF_1 and RF_2 are provided by two vector network analyzers (VNA_1 and VNA_2) (Agilent B722ES, Keysight E5063A). Then the two RF signals are amplified by two electrical amplifiers (EA_1 and EA_2), respectively. The $HC_{1,2}$ (RF-Lambda RFHB05G26GVK) converts $RF_{1,2}$ into two orthogonal signals. Both of the DMZMs are biased at the quadrature transmission point to implement SSB+C modulation. The measured extinction ratio of each sub-DMZM is more than 20 dB. The output power of the EDFA (Conquer KG-EDFA-P) is about 10.8 dBm. The FD-OP (Finisar WaveShaper 4000s), with a 1-GHz programmable resolution, adds same phase shifts and attenuation to two orthogonal polarization directions. The 1-GHz frequency resolution is sufficient to shift the phase of a microwave signal in a full 360° range [16], [17]. After 2-OSBs phase processing by the FD-OP, the light injects into a PD (Optilab PD-30) with a working band over 60 kHz-32 GHz.

Fig. 3 shows the measured optical spectra after the FD-OP along x- and y- directions when $\varphi = 3\pi/4$. During the measurement, RF_1/RF_2 is set at 13 GHz/24.5 GHz with an output power of -15 dBm/-5 dBm. After EA_1/ EA_2, RF_1/RF_2 is measured to be 10.4 dBm/7.5 dBm. The
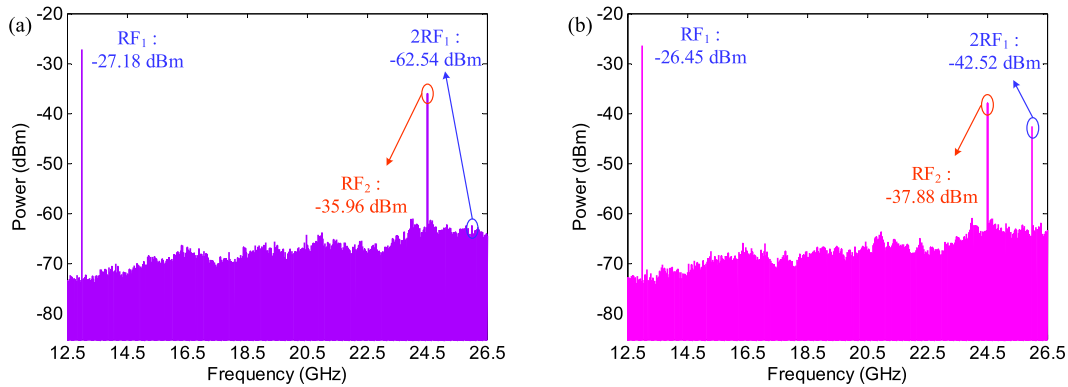
Fig. 4. Electrical spectra of (a) the proposed and (b) conventional FD-OP-based phase shifter with a 13 GHz and 24.5 GHz input.
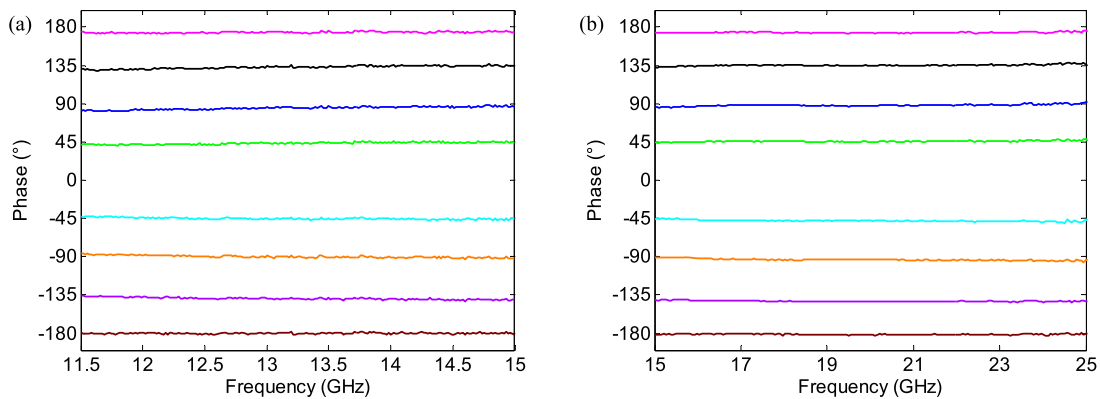

Fig. 5. Phase-frequency response along (a) x- and (b) y- directions for different phase shifts.

+1-OSBs (in terms of frequency rather than wavelength) are over 23 dB lower than the corresponding −1-OSBs due to SSB+C modulation. A strong −2-OSB of RF_1, which will lead to SHD after beating with the carrier in PD, is observed to be close to the −1-OSB of RF_2. Fig. 4(a) shows the recovered electrical spectra measured by an electrical signal analyzer (Agilent EXA N9010A). The SHD of RF_1, with its power as low as −62.54 dBm, is close to the fundamental of RF_2. The electrical spectra of the conventional FD-OP-based phase shifter that without −2-OSBs phase processing [16] is also measured, as shown in Fig. 4(b). The SHD is measured to be only 4.64 dB lower than RF_2, which leads to a low SNR. Thanks to SSB+C modulation and 2-OSBs phase processing, the 26-GHz SHD is reduced by 20.02 dB while the fundamental power is almost unchanged. From Fig. 4, RF_2 has a lower conversion gain compared with RF_1. This is because the modulator and PD are of lower amplitude responses at higher frequencies. Furthermore, the electric cables also suffer from larger insertion loss at higher frequencies.

Figs. 5(a) and 5(b) show the phase-frequency response along x- and y- directions measured by VNA_1 and VNA_2, respectively. Flat 360° phase shifts within 11.5-25 GHz with a step of 45° are achieved by programing the FD-OP. Figs. 6(a) and 6(b) show the corresponding amplitude-frequency response along x- and y- directions, respectively. The amplitudes are frequency-dependent and phase-dependent because of the finite slope for the FD-OP amplitude and phase responses [17]. The power variation is less than 3 dB over 11.5-13.5 GHz and less than 2 dB over 13.5-25 GHz. The acceptable variation can be further compensated by programing the FD-OP amplitude response or using a variable optical attenuator. Besides, phase- and
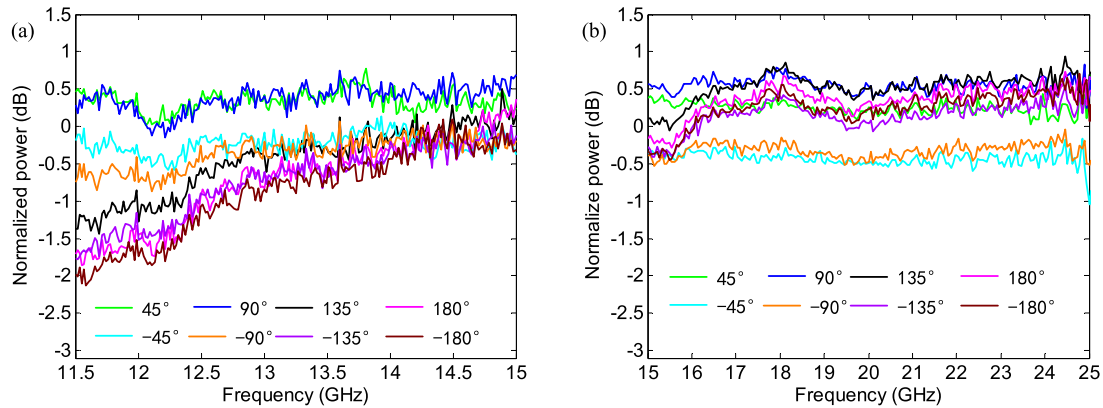
Fig. 6. Amplitude-frequency response along (a) x- and (b) y- directions for different phase shifts.
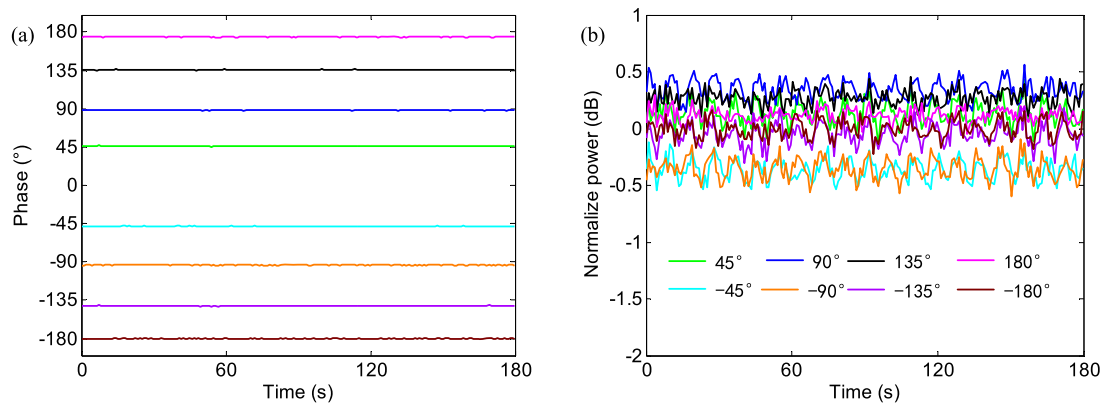

Fig. 7. Long-term (a) phase stability and (b) amplitude stability at 17 GHz.

amplitude- imbalance of the HCs and DC drift of DMZMs also contribute to the acceptable frequency-dependent phase-frequency response and amplitude-frequency response.

The long-term stability of the proposed phase shifter at 17 GHz is also measured by sweeping the time from 0s to 180s, as shown in Fig. 7. The long-term maximum phase/power fluctuation is only 1.49°/0.57 dB, which is very stable.

To further investigate the SDs suppression, a two-tone RF signal with the frequencies of 12.4 GHz and 12.6 GHz generated by two VNAs is added to $DMZM_1$. During the two-tone measurement, RF_2 is turned off due to the lack of another signal generator. Accordingly, $DMZM_2$ is biased at the minimum transmission point to reduce the power of the optical carrier injected into the PD. Fig. 8(a) shows the recovered RF signals when the two-tone powers are both 10.4 dBm and φ is changing from $-\pi$ to π with a step of $\pi/4$. After 2-OSBs phase processing, the IMD2 at 25 GHz is as low as -75.71 dBm. As a comparison, the measured electrical spectra of the conventional FD-OP-based phase shifter are shown in Fig. 8(b). The power of the IMD2 is up to -53.59 dBm, which is higher than IMD3. If RF_2 is still applied to the $DMZM_2$, a 24.5-GHz fundamental signal will be observed, as shown in Fig. 8. The SDs are close to RF_2, which will limit the system performance. Thanks to 2-OSBs phase processing, the proposed phase shifter suppresses the IMD2 by 22.12 dB. Besides, the IMD2 is lower than the IMD3 after 2-OSBs phase processing, resulting in an improved system performance.

The measured SFDR of the proposed and conventional FD-OP-based phase shifter is shown in Fig. 9. In conventional FD-OP-based phase shifter, SDs are dominant compared with IMD3 when input power is lower than 15.8 dBm. After 2-OSBs phase processing, the $SFDR_2$ is improved by
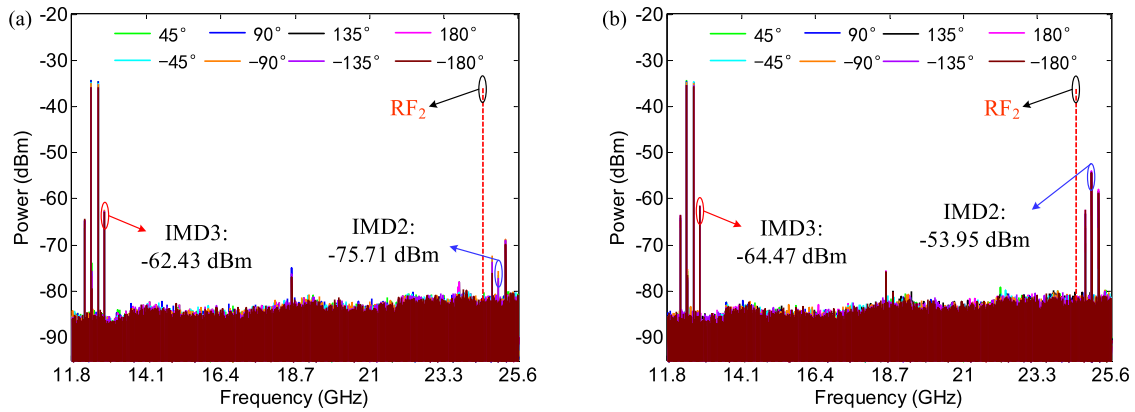
Fig. 8. Two-tone electrical spectra of (a) the proposed and (b) conventional FD-OP-based phase shifter for different phase shifts.
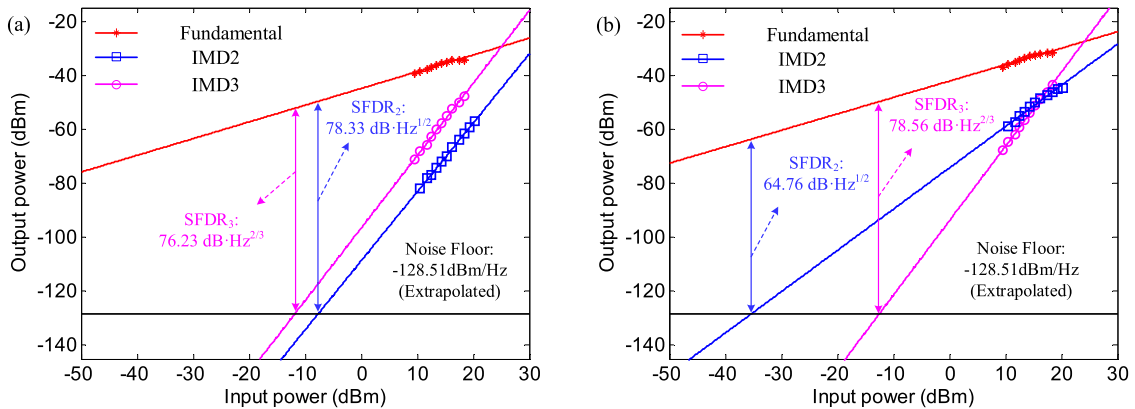

Fig. 9. SFDR of (a) the proposed and (b) conventional FD-OP-based phase shifter.

13.57 dB from 64.76 dB·Hz$^{1/2}$ to 78.33 dB·Hz$^{1/2}$, while the SFDR$_3$ is almost unchanged. Owing to 2-OSBs phase processing, the system performance is limited by IMD3 instead, leading to an improved threshold of SFDR. The slope of the SFDR$_2$ is changed from 2 to 3, whose reasons are explained as follows. Firstly, the powers of ±2-OSB are not equal in the experiment, which is shown in Fig. 3. This is due to the phase and amplitude imbalance of HC$_{1,2}$ and DC drift of DMZM$_{1,2}$. The power imbalance of ±2-OSB leads to reduced performance of IMD2 suppression. Secondly, +1-OSB and +3-OSB are not effectively suppressed, as shown in Fig. 3. It also leads to reduced performance of IMD2 suppression. Therefore, the slope of the SFDR$_2$ is between 2 and 4. The measured noise floor is −128.51 dBm/Hz. The noise floor depends on the RF signals quality. The RF signals quality generated by VNAs is not as good as ones generated by conventional analog signal generators (ASGs), and the EAs furthermore raise the noise floor. In addition, strong relative intensity (RIN) noise of the LD and amplifier spontaneous emission (ASE) noise of the EDFA also raise the noise floor. The improved SFDR$_2$ of the phase shifter can be further enhanced by using a high-performance LD [26] and two ASGs.

The only electronic device required for the proposed photonic link is the HC which will limit the maximum operational frequency of the phase shifter. The maximum operational frequency can be easily increased using a HC with a larger working band. At present, wideband commercial HC (Marki QH-0867) has an operational frequency up to 67 GHz. It has a power/phase imbalance of ±0.6 dB/±6°, which has little influence on the system performance. The minimum operational frequency of the proposed phase shifter can be as low as 4 GHz, but large power fluctuation will

be observed due to the finite slope for the FD-OP phase response [17], [27]. As a remedy, power compensation is needed in lower frequencies. With a 11.5-GHz lowest input RF frequency in our experiments, the proposed shifter has a highest frequency up to 34.5 GHz according to theoretical analysis in Section 2. The theoretical bandwidth of the proposed phase can be easily expanded by increasing the lowest input RF frequency. Due to experimental limitations of our lab, only a 25-GHz highest operational frequency is demonstrated. Furthermore, multiple independent phase shifting channels can be obtained by adding optical sources with different wavelength [16], [27], [28].

4. Conclusions

In conclusion, a photonics-assisted super-octave microwave phase shifter with 360° phase shifts is proposed and experimentally demonstrated. The proposed phase shifter is implement using techniques of polarization interleaving and 2-OSBs phase processing. Less than 3-dB power variation and excellent long-term stability is demonstrated. After 2-OSBs phase processing by FD-OP, the $SFDR_2$ is improved by 13.57 dB compared with the conventional FD-OP-based phase shifter. Owing to the SDs suppression, the proposed phase shifter is promising for applications in future high-frequency super-octave photonic links.

Acknowledgment

References

[1] Y. Liu, J. Yao, and J. Yang, "Wideband true-time-delay unit for phased array beamforming using discrete-chirped fiber grating prism," *Opt. Commun.*, vol. 207, pp. 177–187. Jun. 2002.
[2] Y. Chen, A. Wen, Y. Chen, and X. Wu, "Photonic generation of binary and quaternary phase-coded microwave waveforms with an ultra-wide frequency tunable range," *Opt. Exp.*, vol. 22, no. 13, pp. 15618–15625, Jun. 2014.
[3] C. Zhang *et al.* "A tunable microwave photonic filter with a complex coefficient based on polarization modulation," *IEEE Photonics J.*, vol. 5, no. 5, Oct. 2013.
[4] Y. Zhang and S. Pan, "Broadband microwave signal processing enabled by polarization-based photonic microwave phase shifters," *IEEE J. Quantum Elect.*, vol. 54, no. 4, Aug. 2018.
[5] S. Pan and J. Yao, "Photonics-based broadband microwave measurement," *J. Lightwave Technol.*, vol. 35, no. 16, pp. 3498–3513, Aug. 2017.
[6] Y. Tousi and A. Valdes-Garcia, "A Ka-band digitally-controlled phase shifter with sub-degree phase precision," *IEEE Radio Freq. Integr. Circuits Symp.*, pp. 356–359, 2016.
[7] H. Lee, S. Moon, Moon. Lee, and J. Yu, "K-band reflection-type phase shifter using phase-shift range enhancement technique," *J. Electromagn. Wave.*, vol. 27, no. 16, pp. 2135–2144, Sep. 2013.
[8] S. K. Koul and S. Dey. "K-band 4-bit phase shifter using two back to back MEMS SP16T switching networks," *J. Microelectromech. S.*, vol. 27, no. 4, pp. 643–655, Aug. 2018.
[9] A. K. Sharma, A. K. Gautam, P. Farinelli, A. Dutta, and S. G. Singh, "A Ku band 5 bit MEMS phase shifter for active electronically steerable phased array applications," *J. Micromech. Microeng.*, vol. 25, no. 3, pp. 35014–35025, Feb. 2015.
[10] M. Pagani, D. Marpaung, and B. J. Eggleton, "Ultra-wideband RF photonic phase shifter with 360° tunable phase and configurable amplitude response," *Int. Topical Meeting Microw. Photon.*, pp. 385–388, 2014.
[11] W. Liu, W. Li, and J. Yao, "An ultra-wideband microwave photonic phase shifter with a full 360 phase tunable range," *IEEE Photonics Technol. Lett.*, vol. 25, no. 12, pp. 1107–1110, Jun. 2013.
[12] W. Li, W. Sun, W. Wang, and N. Zhu, "Optically controlled microwave phase shifter based on nonlinear polarization rotation in a highly nonlinear fiber," *Opt. Lett.*, vol. 39, no. 11, pp. 3290–3293, Jun. 2014.
[13] E.H.W. Chan, W. Zhang, and R. A. Minasian, "Photonic RF phase shifter based on optical carrier and RF modulation sidebands amplitude and phase control," *J. Lightw. Technol.*, vol. 30, no. 23, pp. 3672–3678, Dec. 2012.
[14] S. Pan and Y. Zhang, "Tunable and wideband microwave photonic phase shifter based on a single-sideband polarization modulator and a polarizer," *Opt. Lett.*, vol. 37, no. 21, pp. 4483–4485, Nov. 2012.
[15] W. Zhang and J. Yao, "Ultra wideband RF photonic phase shifter using two cascaded polarization modulators," *IEEE Photonics Technol. Lett.*, vol. 26, no. 9, pp. 911–914, May 2014.
[16] X. Yi, Thomas X., H. Huang, and R. A. Minasian, "Photonic beamforming based on programmable phase shifters with amplitude and phase control," *IEEE Photonics Technol. Lett.*, vol. 23, no. 18, pp. 1286–1288, Sep. 2011.
[17] J. Yang, E. H. W. Chan, X. Wang, and X. Feng, "Broadband photonic microwave phase shifter based on controlling two RF modulation sidebands via a Fourier-domain optical processor," *Opt. Exp.*, vol. 23, no. 9, pp. 12100–12110, May 2015.

[18] J. Capmany and D. Novak, "Microwave photonics combines two worlds," *Nat. Photonics*, vol. 1, no. 6, pp. 319–330, Jun. 2007.

[19] W. K. Burns, G. K. Gopalakrishnan, and R. P. Moeller, "Multi-octave operation of low-biased modulators by balanced detection," *IEEE Photon. Technol. Lett.*, vol. 8, no. 1, pp. 130–132, Jan. 1996.

[20] Y. Gao, A. Wen, Z. Peng, and Z. Tu,"Analog photonic link with tunable optical carrier to sideband ratio and balanced detection," *IEEE Photonics J.*, vol. 9, no. 2, pp. 1–10, Apr. 2017.

[21] Z. Chen *et al.*, "SFDR enhancement in analog photonic links by simultaneous compensation for dispersion and nonlinearity," *Opt. Exp.*, vol. 21, no. 18, pp. 20999–21009, Sep. 2013.

[22] P. S. Devgan, J. F. Diehl, V. J. Urick, C. E. Sunderman, and K. J. Williams, "Even-order harmonic cancellation for off-quadrature biased Mach-Zehnder modulator with improved RF metrics using dual wavelength inputs and dual outputs," *Opt. Exp.*, vol. 17, no. 11, pp. 9028–9039, May 2009.

[23] D. Zhu, J. Chen, and S. Pan, "Multi-octave linearized analog photonic link based on a polarization-multiplexing dual-parallel Mach-Zehnder modulator," *Opt. Exp.*, vol. 24, no. 10, pp. 11009–11016, May 2016.

[24] S. Ishimura, H. Kim, Y. C. Chung, and M. Suzuki, "Broadband IF-over-fiber transmission with parallel IM/PM transmitter overcoming dispersion-induced RF power fading for high-capacity mobile fronthaul links," *IEEE Photonics J.*, vol. 10, no. 1, pp. 1–9, Feb. 2018.

[25] G. Baxter *et al.*, "Highly programmable wavelength selective switch based on liquid crystal on silicon switching elements," in *Proc. Optical Fiber Commun. Conf.*, OSA, 2006.

[26] D. Marpaung, C. Roeloffzen, A. Leinse, and M. Hoekman, "A photonic chip based frequency discriminator for a high performance microwave photonic link," *Opt. Exp.*, vol. 18, no. 26, pp. 27359–27370, Dec. 2010.

[27] X. Yi, L. Li, Thomas X., H. Huang, and R. A. Minasian, "Programmable multiple true-time-delay elements based on a Fourier-domain optical processor," *Opt. Lett.*, vol. 37, no. 4, pp. 608–610, Feb. 2012.

[28] X. Gao *et al.*, "Generating the orbital angular momentum of radio frequency signals using optical-true-time-delay unit based on optical spectrum processor," *Opt. Lett.*, vol. 39, no. 9, pp. 2652–2655, May 2014.